energies

MDPI

Article

A Universal PSpice Simulation Model of a Switched Buck Voltage Regulator

Dobroslav Kováč *, Tibor Vince *, Matej Bereš *, Ján Molnár, Jozef Dziak, Patrik Jacko and Irena Kováčová

Department of Theoretical and Industrial Electrical Engineering, Technical University Kosice, Park Komenskeho 3, 042 00 Kosice, Slovak Republic

* Correspondence: dobroslav.kovac@tuke.sk (D.K.); tibor.vince@tuke.sk (T.V.); matej.beres@tuke.sk (M.B.)

Abstract: The article describes the design of a universal simulation model of a voltage regulator for applications compatible with the globally used PSpice program. Users can create a model of any type of integrated switching voltage regulator that is currently available on the market by setting its individual parameters. The proposed connection of the regulator was applied in the connection of the buck DC–DC converter. The accuracy of the model was verified by comparing the results obtained by the simulation to other official models and to practical measurements taken on a real sample of the converter. The versatility of the model was proven by comparison with another type of converter with different parameters.

Keywords: PSpice simulation model; switching voltage regulator; buck DC–DC converter

check for updates

Citation: Kováč, D.; Vince, T.; Bereš, M.; Molnár, J.; Dziak, J.; Jacko, P.; Kováčová, I. A Universal PSpice Simulation Model of a Switched Buck Voltage Regulator. *Energies* **2022**, *15*, 8209. https://doi.org/10.3390/en15218209

Academic Editor: Alon Kuperman

Received: 3 October 2022
Accepted: 20 October 2022
Published: 3 November 2022

Publisher's Note: MDPI stays neutral with regard to jurisdictional claims in published maps and institutional affiliations.

Copyright: © 2022 by the authors. Licensee MDPI, Basel, Switzerland. This article is an open access article distributed under the terms and conditions of the Creative Commons Attribution (CC BY) license (https://creativecommons.org/licenses/by/4.0/).

1. Introduction

The use of power semiconductor converters in common practice has currently become a matter of course. One of the many areas where they are applied is the conversion of DC supply voltage to DC voltage with other parameters. Different types of DC–DC converter connections are used for this purpose, for instance, to achieve lower output voltage with lower current and voltage ripple [1–3], and in other cases, where different control strategies are used [4–6], and special topologies [7,8] to achieve better results. The most used connection is probably the buck converter connection [9]. Various manufacturers of semiconductor components have focused on the development and production of different types of switching voltage regulators [10–15]. The basic topology of such a buck converter supplemented with several external components is shown in Figure 1. This basic topology contains mandatory electrical components [16] to operate the regulator properly.

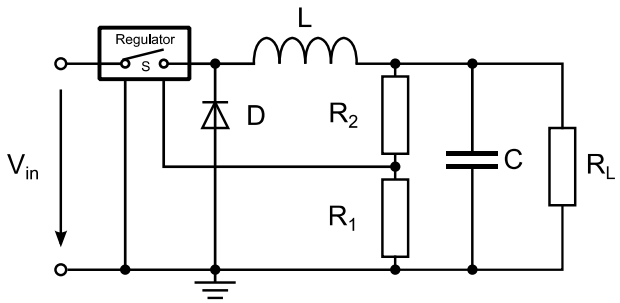


Figure 1. Connection of a buck converter with a switched voltage regulator.

The main purpose of such a voltage regulator, aside from regulating output voltage, is power switching with a specific frequency and with the maximum input voltage and current that can be handled [17,18]. Thus, if more power is needed, the manufacturer

recommends buying a more expensive regulator, and in many cases, a more powerful voltage regulator is purchased. However, when handling power of several hundreds of watts, another solution can be much more suitable. This paper provides several solutions in which more power can be achieved with the use of a low-power voltage regulator and several additional electrical components. Before providing any solution at all, however, the regulator model should be first explained.

2. Regulator Model

Most integrated switching voltage regulators currently available on the market have the following main features and parameters:

- An input supply voltage terminal V_{in}, which is usually in a range of up to 40 V, and for higher voltage regulators, the input voltage can be up to 60 V;
- A GND terminal as a negative power supply voltage terminal;
- An ON/OFF terminal, which is a control terminal that can activate or deactivate the operation of the regulator;
- An FB (feedback) terminal to compare output voltage with a fixed built-in reference voltage V_{ref}, which helps to regulate the desired output voltage level;
- An OUT terminal to connect other external components, such as a diode D, an inductor L, a capacitor C, a resistance R etc.;
- Fixed switching frequency f;
- Built-in current protection for the internal power switch of the regulator with the value I_{max};
- The specified amount of current I_Q, which is taken by the regulator chip itself from the power supply;
- Specified amount of voltage drop V_{sat} on the regulator, at maximum current and switch S closed;
- Entered maximum duty factor D_{max};
- Specified range of resistance values of resistor R1 (according to Figure 1).

For the designed model of the controller to be universal, it must be able to reflect all the above-mentioned properties and parameters. Based on that, it is possible to draw its block diagram shown in Figure 2.

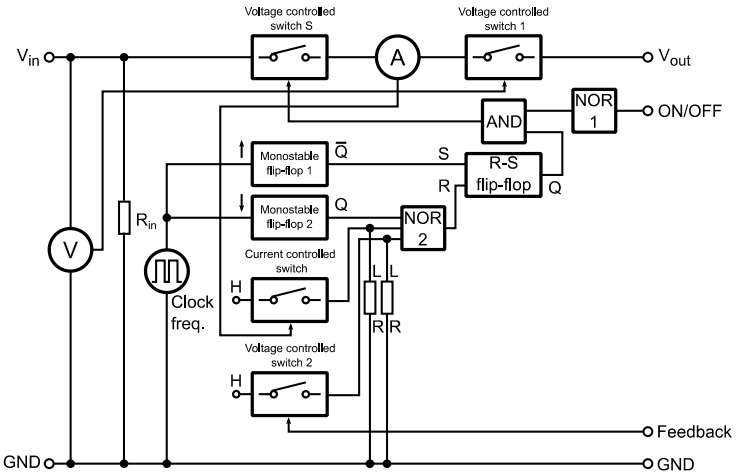


Figure 2. Block diagram of the proposed universal voltage regulator.

The operation of the proposed controller is as follows. The basis is a frequency generator (clock freq.). It generates a rectangular signal with the required switching frequency of the controller and a duty factor equal to D_{max}. The amplitude of the output signal is 5 V due to its further processing using TTL circuits. At the rising edge of its output signal, the monostable flip-flop circuit 1 generates, at its output $\overline{Q}$, a short pulse with a logic

level of L, and the pulse feeds the input S of the R-S flip-flop circuit. This sets its output to a logic H value. If a logic L is present at the ON/OFF input, the logic H is transmitted via the AND gate to the voltage-controlled switch S, which turns on. The closed-state resistance of the switch must be set according to the following relation:

$$R_{sw} = R_{on} = \frac{V_{sat}}{I_{\max}}, \tag{1}$$

In a similar way, the off-state switch resistant R_{off} is given by:

$$R_{off} = \frac{V_{in}}{I_L}, \tag{2}$$

where V_{in} is the value of the supply voltage, and I_L is the value of the output leakage current of the regulator in the off state. A monostable flip-flop 2 is connected to the falling edge of the signal from the frequency generator. It generates a short pulse at its output Q. This pulse is transmitted through the gate NOR2 to the R input of the R-S flip-flop circuit. This flips the R-S circuit to logic L. It also causes the voltage-controlled switch S of the controller to switch off via the AND gate. There are two ways to shorten the maximum pulse duration, either by exceeding the maximum permissible current I_{max} of the regulator or by exceeding the required output voltage. The first case is treated by sensing the current of the switch with ammeter A. If its value exceeds the value I_{max}, the current control switch is switched on. The logic H is applied to the second of the NOR2 inputs. This ensures premature switching of the output of the R-S flip-flop circuit to the logic L before reaching D_{max} and, thus, the duration of the switching pulse shortening. The second case is treated with voltage-controlled switch 2, which is switched when the value of the voltage at the input FB (feedback) exceeds the value of the internal reference voltage V_{ref} of the controller. In this case, the logic H is again applied to the third of the NOR2 inputs and shortens the duration of the switching pulse of the regulator below the value D_{max}. The ensuring of the logic L values at the inputs two and three of NOR2 is realized by a pair of resistors R. Blocking of the controller operation is ensured by a signal fed to the ON/OFF input of the regulator, which is further inverted by member NOR1, whose output is the second input of the *AND* gate. If the value of logic H at the ON/OFF input is exceeded, it is inverted to the level of logic L via *NOR1.* The transmission of control signals for the voltage-controlled switch S through the AND gate is blocked. The simulation of the internal current consumption I_Q of the regulator is realized by means of the resistor R_{int}, the value of which is given by the ratio:

$$R_{\text{int}} = \frac{V_{in}}{I_Q}, \tag{3}$$

where V_{in} is the supply voltage and I_Q is the supply current of the controller. Exceeding the supply voltage V_{in} leads to a break in the switch on the real component and usually disconnects the circuit. The task of this fact is to simulate voltage-controlled switch 1. It is opened by exceeding the value V_{in} sensed by the voltmeter V above the value V_{max}.

In order to implement the proposed model of a universal voltage regulator, it is advantageous to use the widely used PSpice program [19] or one of its equivalents. In our case, this is a TINA program [20] (Toolkit for interactive network analysis). The program library can be supplemented in the form of a subcircuit based on the PSpice program rules [21–23].

PSpice software is a widely used and accepted standard for many electrical circuit simulation software [24,25]. Many producers offer a spice model for their products. In order to make the sub-circuit more user-friendly, it is possible to covert text notation in the graphic form using regulator graphics symbols. Only variable parameters would be editable by the user. In our case, this was the following parameters: f, V_{ref}, I_{max}, R_{sw}, D_{max}, V_{max}, and R_{int}. Since each real regulator is individual, the triggering of their oscillators is random. Therefore, we added the Delay parameter to the model. The user can set

individual modes of the regulator's time operation even in the case of multiple uses in one connection. The text notation of the universal model is presented in Appendix A.

The integrated switching voltage regulator LM2576 serves to show a graphical presentation of the model. An interactive dialog box allowing the main parameters of the model to be changed in the graphical presentation of the model is shown in Figure 3.

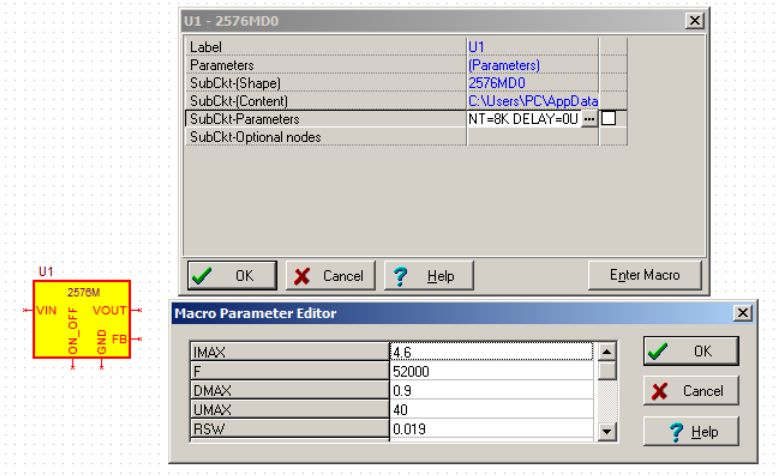


Figure 3. Graphic symbol and property windows of the LM2576 switched voltage regulator model in the TINA program.

The LM2576 controller using the catalog parameters was chosen for the first proof of the correct operation of the proposed simulation model. The output voltage of the converter with the given regulator can be calculated from the relation [14]:

$$V_{out} = V_{ref}(1 + \frac{R_2}{R_1}), \tag{4}$$

where V_{ref} has a value of 1.23 V. The circuit was supplemented by external components with the values recommended by the manufacturer: L = 100 µH, R_5 = 460 mΩ, V_{in} = 40 V, R_1 = 2 kΩ, R_2 = 22.39 kΩ, C_1 = 100 µF, C_2 = 1 mF, and Rc = 181 mΩ. The SD1 diode was selected as MBR360. The load resistor has a value of R_L = 5 Ω. The overall connection of the inverter with the controller model and external components is shown in Figure 4. The resulting waveforms obtained by the simulation are shown in Figure 5.

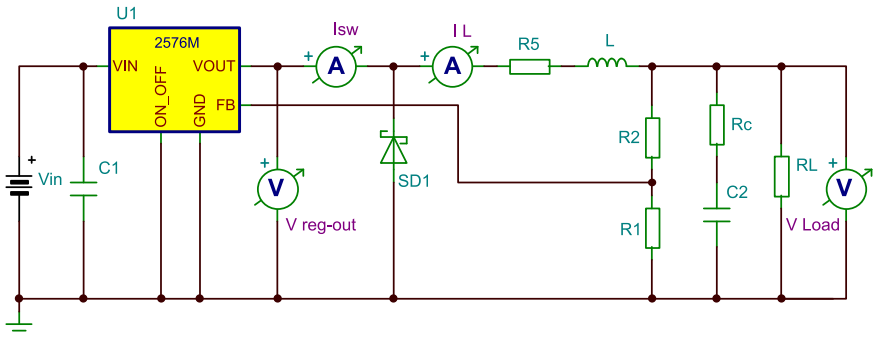


Figure 4. Electrical wiring diagram of the buck DC–DC converter with the LM2576 regulator model.

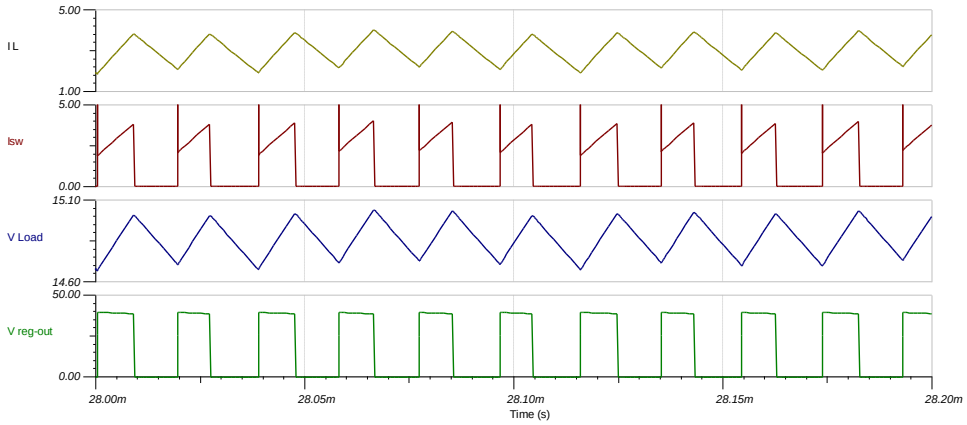
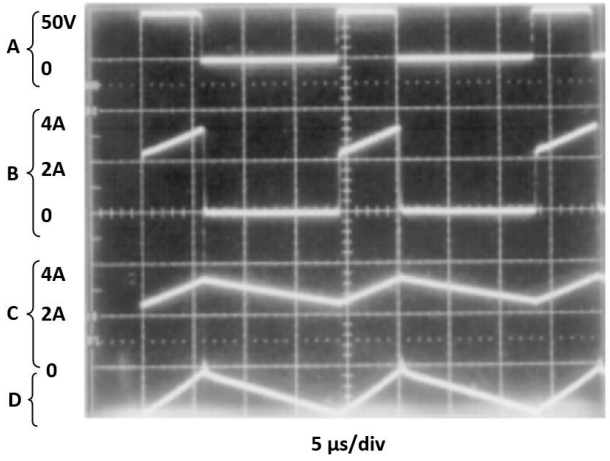


Figure 5. Graph curves of the quantities of the investigated converter obtained by simulation in the TINA program.

Validation of the correct operation of the converter can be performed by comparing the results obtained by the simulation with the results obtained by the measurement showed in Figure 6, which is stated by the manufacturer in the datasheet for the component [14].



V_{OUT} = 15 V
A: Output Pin Voltage, 50 V/div
B: Output Pin Current, 2 A/div
C: Inductor Current, 2 A/div
D: Output Ripple Voltage, 50 mV/div,
AC-Coupled
Horizontal Time Base: 5 µs/div

Figure 6. Measured main values of the converter obtained from the LM2576 datasheet.

In addition to the static activity verification, it is also necessary to verify the reliability and fidelity of the model during the dynamic operation. This can be performed by comparing the waveforms obtained by the simulation and the waveforms measured by the manufacturer [14]. The analyzed circuit is shown in Figure 7. The values of the circuit elements are the same as the circuit in Figure 4. Only the load resistance RL2 with a value of 32.5 Ω was added. The results obtained by the simulation are shown in Figure 8, and the catalog curves are shown in Figure 9.

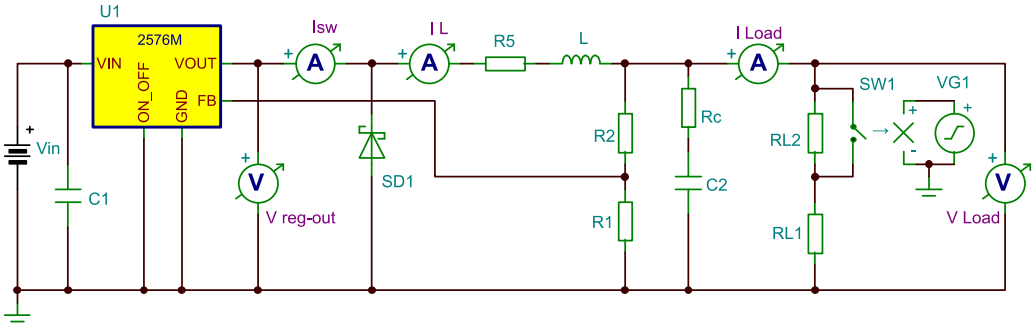


Figure 7. Wiring diagram of the investigated circuit in the TINA program.

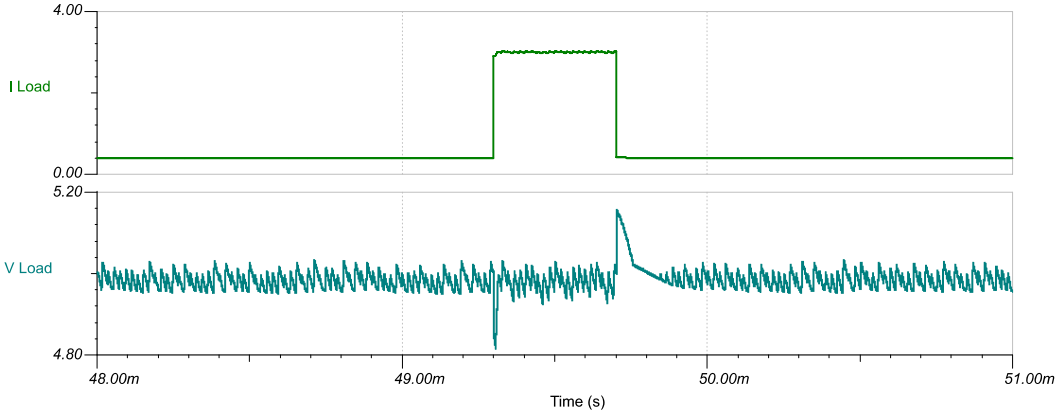


Figure 8. Main graph curves of the converter model with LM2576 regulator during its dynamic operation obtained by simulation.

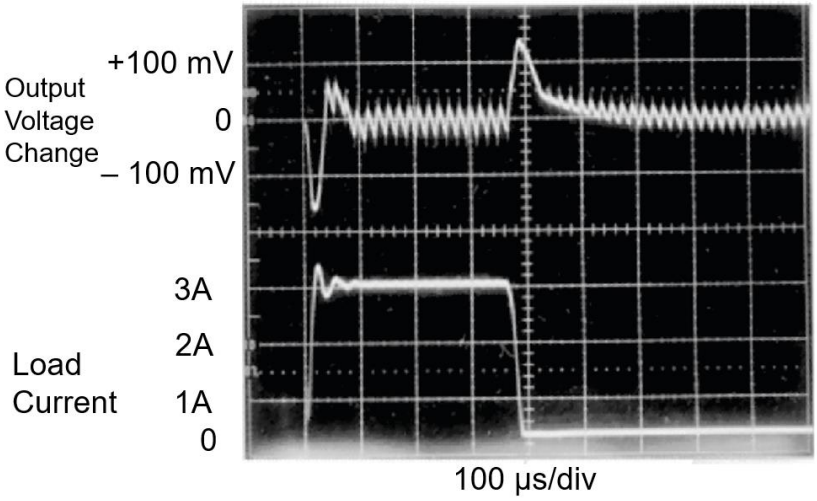


Figure 9. Main graph curves of the converter with the LM2576 regulator during its dynamic operation obtained from the regulator datasheet.

The model sufficiently corresponds to the real component in a static state (Figure 5 vs. Figure 6) and a dynamic state (Figure 8 vs. Figure 9) when comparing model results and data given by the manufacturer. Based on this, the model can be further used to investigate the behavior of a newly designed circuit.

3. Universal Model Comparing with Existing LM 2576HV PSpice Models and a Real 2576HV

There is no other universal buck DC–DC converter model found on the Internet. There are, of course, general buck DC–DC converter schematics, but none of them has an

implementation of the variable properties such as switching frequency, current and voltage limitations, feedback voltage, etc. In order to determine universal model accuracy, it was compared with official PSpice models and with the real item. A standard LM2576 converter was out of stock in all the relevant shops—possibly due to the semiconductor component crisis—so the closest alternative, an LM2576HV from Texas Instruments, was chosen. Texas Instruments (TI) offers official PSpice models for many of their products, including the LM2576HV; therefore, the universal model could be compared with the model officially provided by the manufacturer. The real DC–DC converter based on the TI LM2576HV is shown in Figure 10.

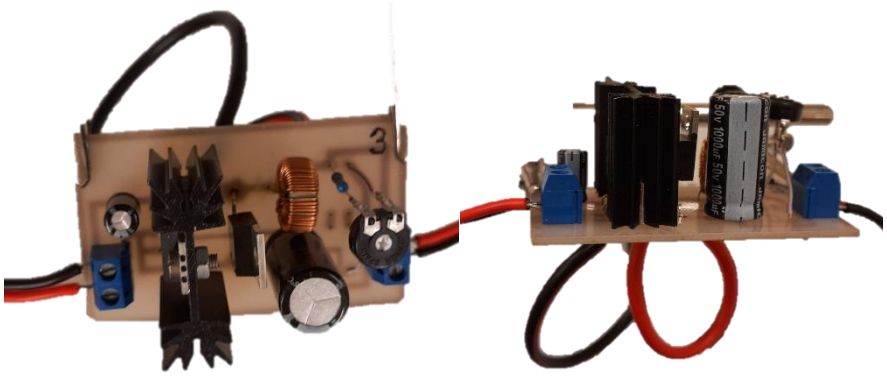


Figure 10. Real LM2576HV DC–DC converter—top (**left**) and side (**right**) view.

The two wire loops that can be seen on the bottom of the PCB are used for current measurement, where current from the switch (I_{sw}) and current through the coil (I_L) (according to Figure 5) are measured. Moreover, other circuits component values from the Figure 4 circuit were updated according to the real component as follows: L = 108 µH, R5 = 103 mΩ, V_{in} = 45 V, R_1 = 3.1 kΩ, R_2 = 9.5 kΩ, C_1 = 100 µF, C_2 = 883 µF, and Rc = 61 mΩ. The SD1 diode was implemented by an MBR1645. The real component's value was measured on a HAMEG HM8118 LCR bridge. The load resistance, including parasite resistance, was calculated from the load voltage and load current measured using an oscilloscope and the resulting resistance value was R_L = 1.79 Ω.

Official PSpice models, including datasheet, were taken from the official product web [11]. Texas instruments offer many products PSpice models. The offered PSpice models can be in the form of an encrypted full PSpice component or an unencrypted PSpice script. Encrypted models can be used in the PSpice application only, whereas unencrypted PSpice script models can also be used in other simulation software supporting the PSpice script, including TINA. Both types of PSpice models are available for the LM2576HV. This allows three models (universal, encrypted, and unencrypted) to be compared with the real LM2576HV converter. The simulation based on the encrypted PSpice model was performed on PSpice-TI [19] software, and simulations based on universal and unencrypted models were performed on TINA-TI software [20]. The circuit components and their values were identical except for the switching regulator model itself. The universal model parameters were updated from the original LM2576 parameter values (Figure 3) to LM2576HV according to the datasheet [26], where new setting values are shown in the Parameter Editor Windows in Figure 11.

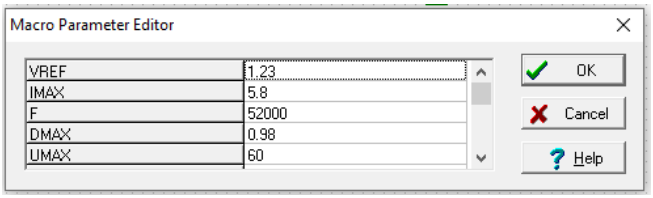


Figure 11. Universal model parameters according to the LM2576HV datasheet.

The real measurement was performed with a Tektronix DPO7354 oscilloscope, and the currents were measured using Tektronix TCP0030 current probes. The measuring laboratory [27] is shown in Figure 12.

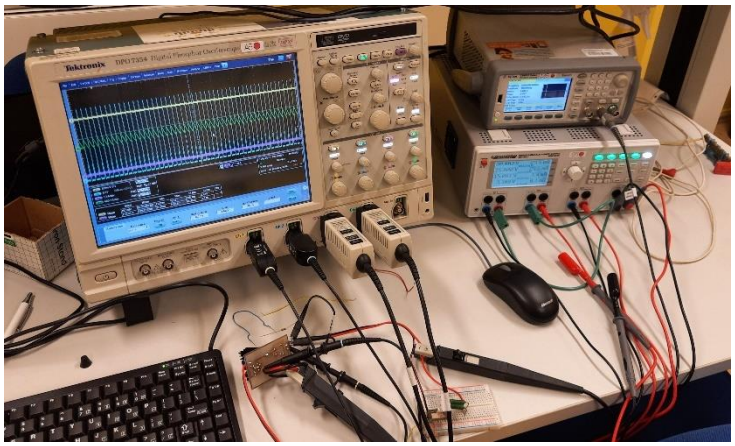


Figure 12. The experimental measurement of the LM2576HV DC–DC converter.

First, the steady-state circuit parameters were compared. The parameters mentioned in Figures 5 and 6 were measured and compared with the simulations. An example of a steady-state measurement is shown in Figure 13.

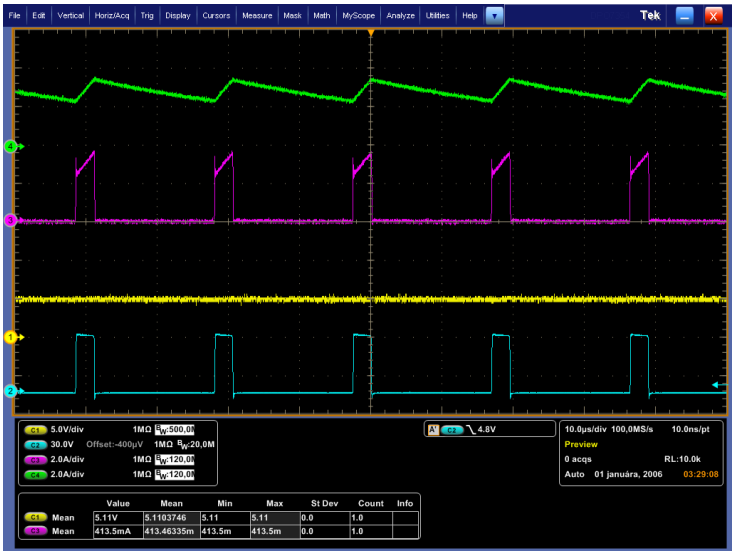


Figure 13. The example of a steady state measurement; Channel 1 (yellow) presents "V Load", Channel 2 (cyan) presents "V reg-out", Channel 3 (purple) presents Isw, and Channel 4 (green) presents I L.

For a better comparison, the measured and simulated values were exported and put together into one graph via MS Excel. This showed that the graph curves are very similar;

therefore, the different details are also shown in the graphs below. A real measurement cannot be performed in a specific time, but in the steady-state repeating graph curves, the specific time is not as important. The time of the first positive edge of the measured $V_{reg\text{-}out}$ signal was synchronized with the first positive edge of the $V_{reg\text{-}out}$ signal of the universal model. In order to make the simulations more effective, parameters (I_{sw}, $V_{reg\text{-}out}$, I_L, V_{Load} from the beginning time (t = 0) were observed. The simulations showed that the transient response on start takes approximately 1.6 ms, and after that, the regulator works on its work point. The curves after 2nd ms were investigated.

First, the voltage from the regulator ($V_{reg\text{-}out}$) comparison is shown in Figure 14, and differences in the details are shown in Figure 15.

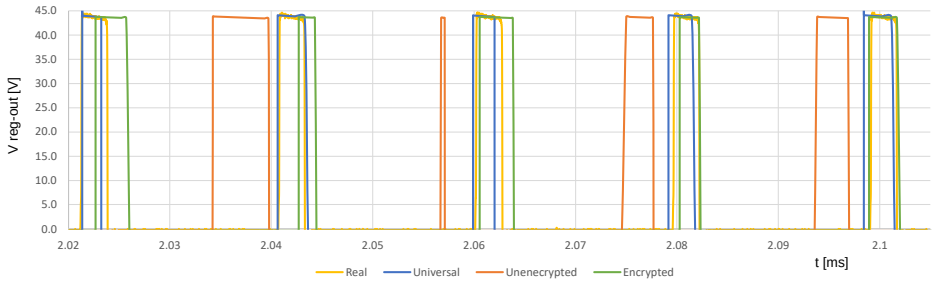


Figure 14. $V_{reg\text{-}out}$ models and real measurement time graph curves.

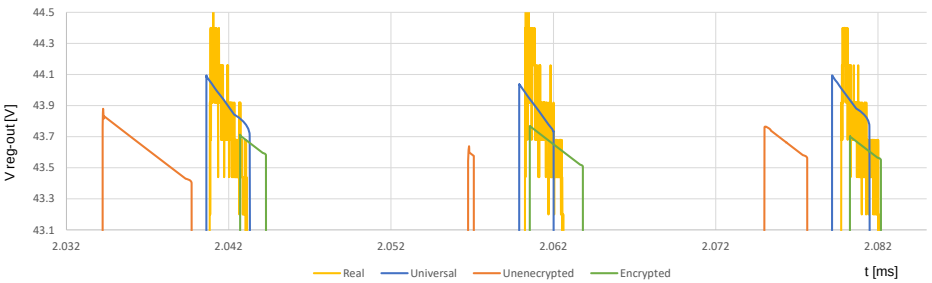


Figure 15. Detailed $V_{reg\text{-}out}$ models and real measurement time graph curves.

Figure 14 shows that all the time graph curves are similar. More significant differences can be seen from an unencrypted model where a certain level of instability can be observed. Generally, the signal from the universal model and encrypted model are very close in shape, amplitude, and frequency to each other and to the measured signal. A more detailed look at the amplitude differences is shown in Figure 15.

The current time course comparison from the regulator (I_{sw}) is shown in Figure 16.

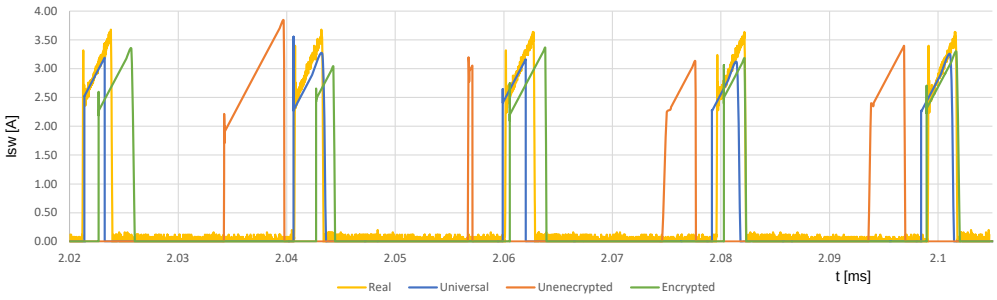


Figure 16. I_{sw} models and real measurement time graph curves.

As can be seen in Figure 16, the impulses are similar to each other. A more detailed illustration is shown in Figure 17. Moreover, the unencrypted model seems to be more unstable compared to the universal and encrypted models.

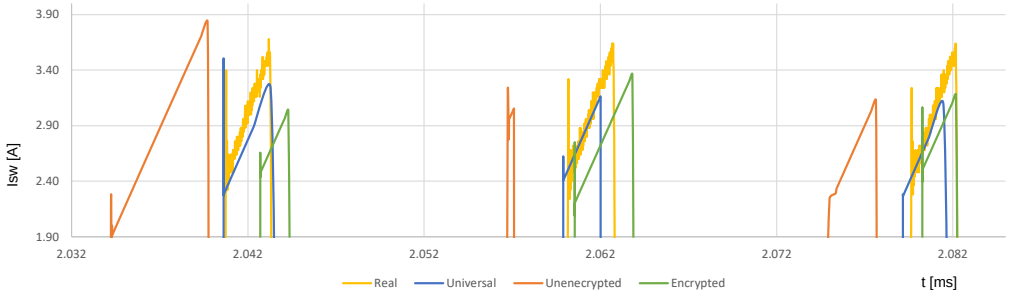


Figure 17. Detailed I_{sw} models and real measurement time graph curves.

The current peaks are not in all pulses in curves calculated by TINA software. The current peaks caused by the Schottky diode capacity are very short (approximately 100 ps). The simulation results were calculated in specific discrete time steps. The reason for missing current peaks in some signal curves is that the TINA software time steps skipped the occurrence of the current peaks. A TINA simulation with a maximum time step of 10 ps would create 10 million values for a 100 µs time simulation.

A comparison of the current course flowing through the coil I_L is shown in Figure 18. The graph curves of universal, encrypted, and measured data are very close to each other with minimal differences.

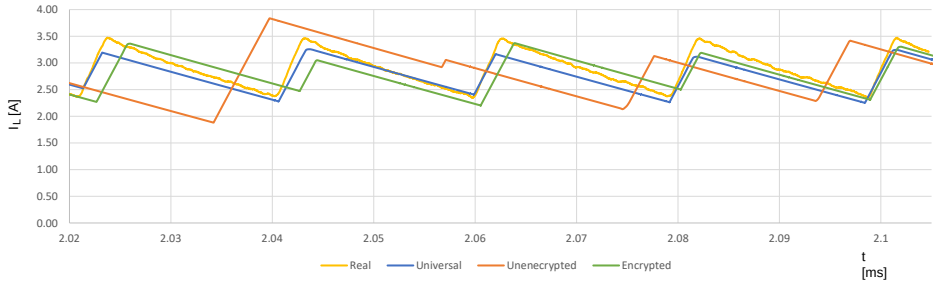


Figure 18. I_L models and real measurement time graph curves.

Details of the coil current graph curves are shown in Figure 19. As can be seen in Figures 18 and 19, the curve of the coil current of the universal regulator model is much more similar to the real measurements and the encrypted model compared to the unencrypted model.

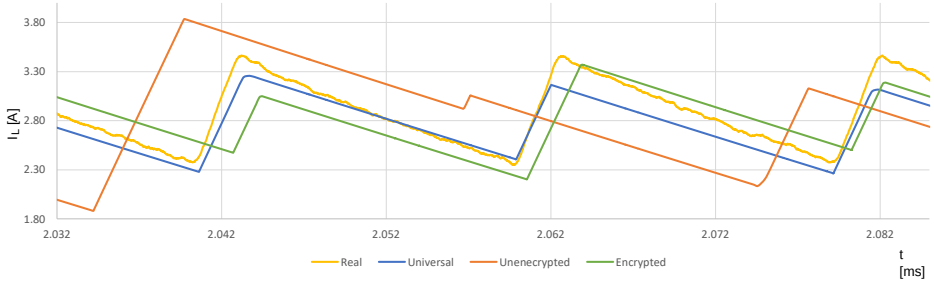


Figure 19. Detailed I_L models and real measurement time graph curves where value of I_L is in Amperes and time is in ms.

The last investigated steady-state parameter on the LM2576HV is the voltage on the load resistor (V_{Load}). The time graph curves for the voltages on the load resistor are shown in Figure 20. As can be seen from the figure, the voltages are very closer to each other. In order to demonstrate the differences in the models, a detailed view is presented in Figure 21.

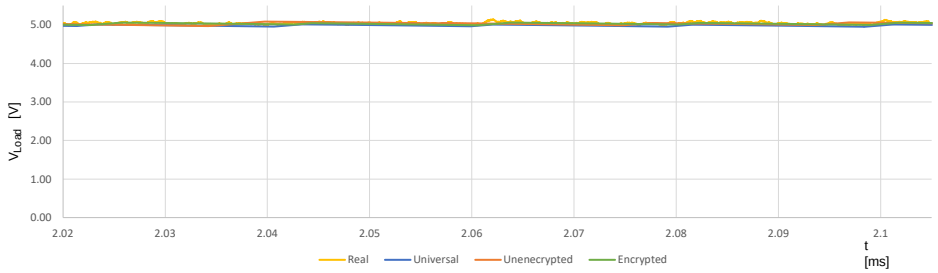


Figure 20. V_{Load} models and real measurement time graph curves.

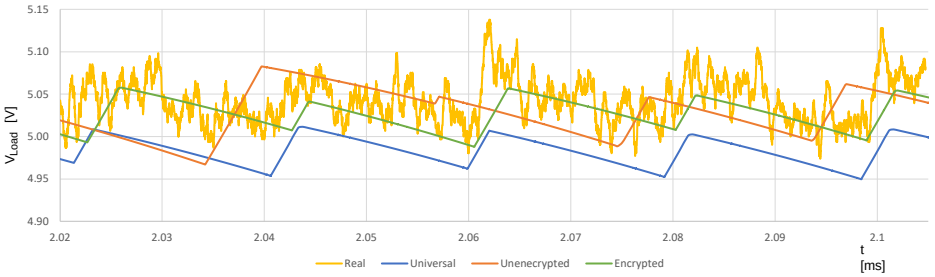


Figure 21. Detailed V_{Load} models and real measurement time graph curves.

The most important parameters to observe are the frequency of the waveforms, voltage ripple (peak-to-peak), waveform shape, and value average. The phase shift between the signals is irrelevant from this point of view. The real measurement waveform is noisy, but it is possible to see the ripple and frequency of the signal when focusing on higher peaks. The average value of the load voltage between the waveforms difference is approximately 0.06 V only, where the universal model has the lowest average, 4.98 V, and the real measured values have the highest average at 5.04 V. The encrypted model average was 5.02 V, and the unencrypted model was 5.028 V. As can be seen from the detailed view, the ripple of other models is optically almost identical, especially when comparing the encrypted and the universal model. As mentioned above, the average load voltage value calculated from the universal model is the lowest, but the real differences are negligible.

Next, the dynamic load behavior was investigated. The circuit was implemented according to Figure 7, where the load R_{L1} was the original 1.79Ω resistor and the second resistor was R_{L2} = 37Ω. In the real measurement, the circuit switch was implemented by the SiC transistor UF3C065030T3S. The signal was generated by an Agilent 33500B Series Waveform Generator. The on-state switch time duration was 500µs. For the dynamic behavior, only the load voltage (V_{Load}) and current (I_{Load}) were investigated.

The V_{Load} response on the load change graph curves is shown in Figure 22. The graph curves are again very close to each other; however, small differences can be seen in the figure. The differences are more obvious in the detailed view in Figure 23.

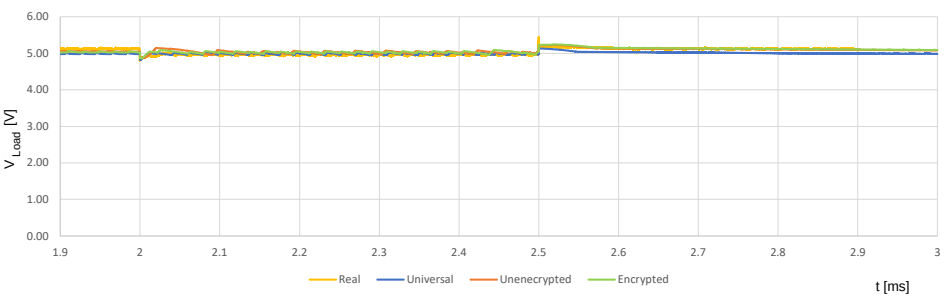


Figure 22. V_{Load} models and real measurement time graph curves on dynamic load.

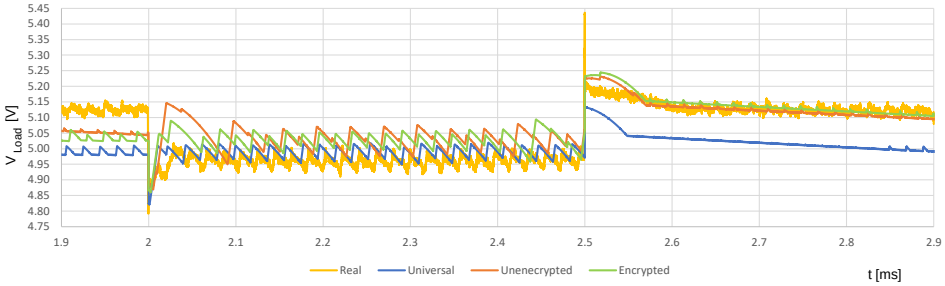


Figure 23. Detailed V_{Load} models and real measurement time graph curves on dynamic load.

The first obvious difference comparing simulations and real measurements is the voltage drop of the real DC–DC converter on the higher load. This voltage drop is caused by the parasitic resistance of the circuit elements, including joints and the electrical conductor. The measured value of the load resistance was R_L = 1.79Ω. This value already included parasite resistance, as mentioned above. This value is thus valid only for the specific load current. The voltage difference between the measured and simulated voltage at the low current is approximately 0.1 V (2%). The goal of the dynamic load state observation is to investigate the time response of the system and voltage ripple change. Moreover, the main goal of the research was to compare the universal model with the existing official models. For this reason, the voltage drop on the parasite resistance differences was not taken into account in the simulations. Another difference is the slightly lower V_{Load} value of the universal model compared to the official models and the real measurement. This behavior was already explored above in Figure 21. In order to investigate the problem, Equation (4) was used to calculate the expected output, and the values of the real resistance were applied. The calculation result is in (5):

$$V_{out} = V_{ref}(1 + \frac{R_2}{R_1}) = 1.23 \times (1 + \frac{9500}{3100}) = 4.999354 \text{ V}, \quad (5)$$

According to calculation (5), when applying the resistance values from the circuit and V_{ref} from the datasheet, the regulated output voltage should be slightly under 5 V. According to this logic, the universal model is the closest to the calculated output voltage. The reason could be that the real converter settings calculate with a voltage drop-down on a higher load. Therefore, the voltage on a low load is a little bit higher. This voltage output shift is probably implemented in both official models. On the other hand, the measured V_{Load} during a high load is almost identical to the universal model simulation.

The current through the load I_{Load} investigation is also very interesting. The I_{Load} time graph curves are shown in Figure 24 and in detail in Figure 25.

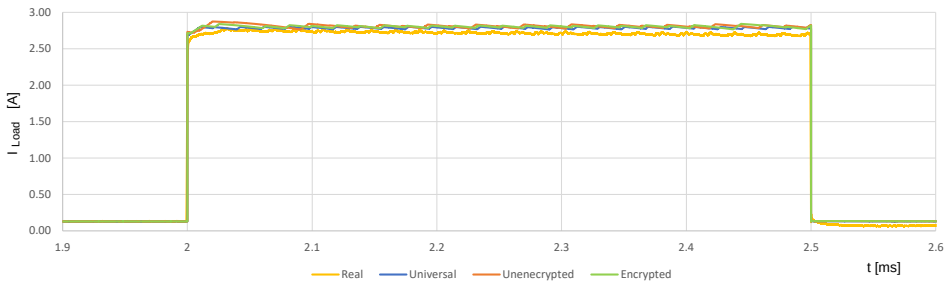


Figure 24. I_{Load} models and real measurement time graph curves in case of dynamic load.

The time graph curves show values very close to each other; however, a measured current drop-down can be observed. This behavior is more obvious in the detailed graph in Figure 25.

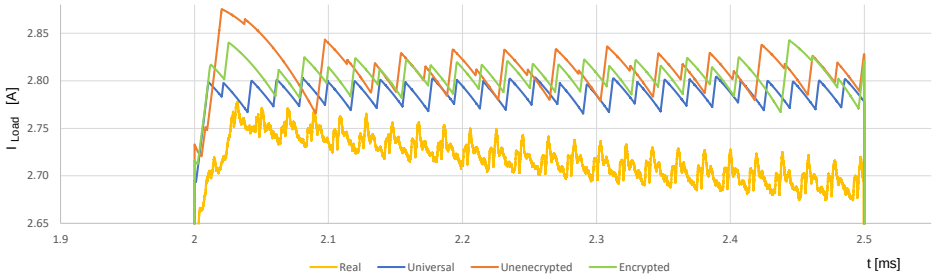


Figure 25. Detailed I_{Load} models and real measurement time graph curves in case of dynamic load.

The current dropdown of the measured course is caused by the Joule heating of the load. Increasing the temperature of the load resistor increases the value of the resistance and decreases the current when at a constant voltage. Other graph curves are very similar with negligible differences. The main complication in comparing simulations and real measurements is the value of the variable circuit—especially the temperature dependence of resistors. The temperature depends on the actual regulator load. The real circuits elements values were measured at room temperature (approx. 23 °C). This problem could be partially compensated by active cooling of the circuit.

The simulations and measurements above showed that if the 2576HV regulator's parameters from the datasheet are applied in the universal model, it can be a full-fledged replacement for the official simulation models provided by the manufacturer. Moreover, the universal model is much closer to the encrypted model and measurement than the official unencrypted model. The unencrypted model shows good average values compared to the measuring, but a closer look at the time curves shows instability in the regulation process.

However, the universal model could have an advantage even over the official encrypted model. The datasheet [11] refers to many parameters with a specific tolerance where the minimum, typical, and maximum value of the parameter is provided. Most of the parameters vary because of the temperature dependent. For instance, the oscillator frequency is typically 52 kHz, but the tolerance is in the range of 47–58 kHz. The current limit is typically 5.8 A, but the tolerance is in the range of 4.2–6.9 A. Feedback voltage is typically 1.23 but may vary in a range of 1.217–1.267 V. The official models most likely have typical values implemented. The universal model is capable of updating these parameters. When a real measurement is performed, the universal model can be tuned up for the specific regulator component in a specific situation (for instance, for higher temperatures, where typical parameter values cannot be guaranteed). In this situation, the universal model would be more precise compared to the official models.

4. Universal Model Comparison with the Official LM2594HV Model

In the third section, we proved that the universal model could be used as a full-fledged PSpice model replacement for the official LM2576HVmodel when parameters from the 2576HV datasheet [26] were applied. A basic comparison to the LM2594HV official model [26] was also made to prove the true universality. The main differences between the previous LM2576HV and LM2596 are that the LM2576 specified output current is 3 A, and it works on a 52 kHz frequency. The LM2594 has specified a 0.5 A output current and works on a 150 kHz frequency. The circuit components' values were taken from the previous steady-state simulations—with the constant load to compare behavior with the previous simulation. The only difference in the circuit parameters was load resistor R_L = 10Ω to achieve the specified 0.5 A output and updated regulator parameters according to the LM2594HV datasheet [28], as Figure 26 shows.

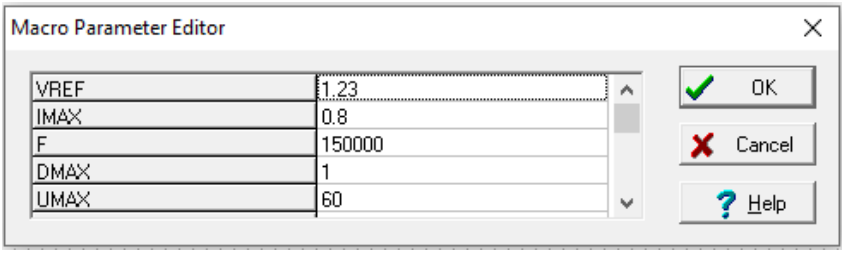


Figure 26. Universal model parameters according to the LM2594HV datasheet.

In order to make the simulations more effective, previous parameters (I_{sw}, $V_{reg\text{-}out}$, I_L, V_{Load}) from the beginning time (t = 0) were observed. The simulations showed that the transient response takes approximately 10.8 ms, and after that, the regulator works on its work point. The reason for the longer time compared to the previous situation is the smaller maximum current of the regulator, and a longer time is required to fill the C2 capacitor (Figure 4) with the desired voltage value. The next 60 µs of the simulation in the PSpice and the TINA were compared after the 11.5 ms.

First, regulator voltage output graph curves are shown in Figure 27. The figure shows that the time graph curves are nearly identical.

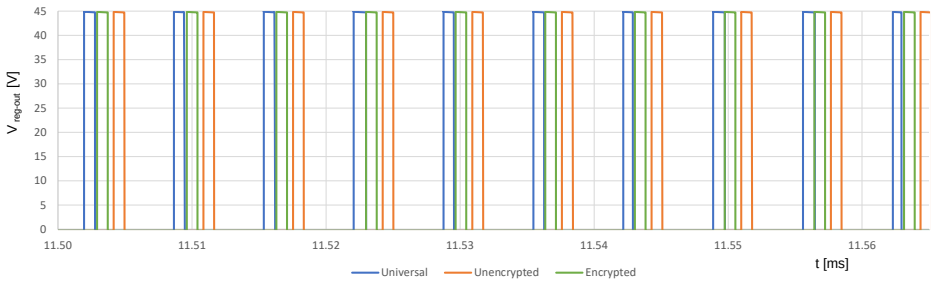


Figure 27. $V_{reg\text{-}out}$ LM2594 models time graph curves.

The current from the switching regulator I_{sw} is shown in Figure 28. The figure shows that the time graph curves are similar in shape and frequency. The real difference is only peaks current and slightly increased maximum of the universal and unencrypted model compared to the encrypted model.

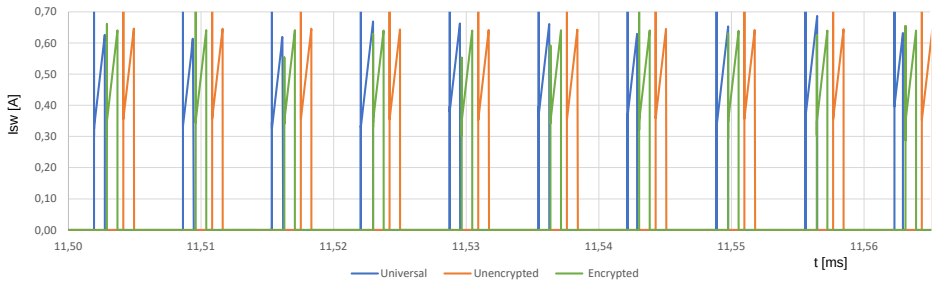


Figure 28. I_{sw} LM2594 models time graph curves.

The current through the coil I_L time graph curves is shown in Figure 29. The curves are again almost identical. The figures show that the officials and universal model results are very close to each other.

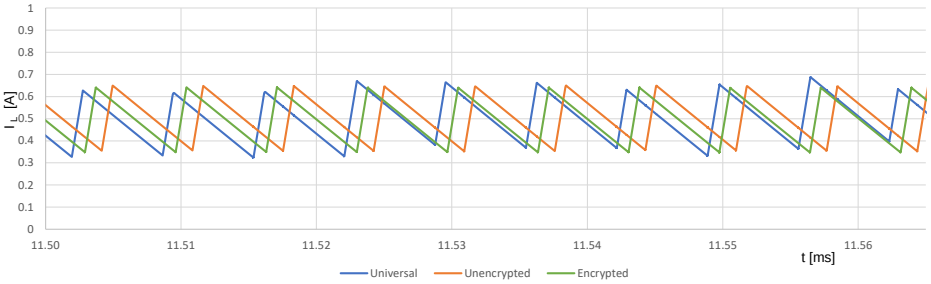


Figure 29. I_L time graph curves using LM2594 regulator.

Finally, the resulting load voltage was compared. The differences are minimal, so a detailed view is presented in Figure 30. The shape, frequency, and calculated load voltage ripple are almost identical. The difference between the official encrypted and the universal model is in absolute value, approximately 60 mV. The difference between the official unencrypted and the universal model is in absolute value, approximately 10 mV only. The universal model load voltage is higher compared to the official models. In the previous LM2576 simulations, this was the opposite. According to the datasheet, the LM2594 has an equal typical feedback voltage of 1.23 V; thus, Equation (5) can be applied. According to (5), the resulting load voltage was slightly below 5 V. Therefore, the universal model is again closer to the expected value.

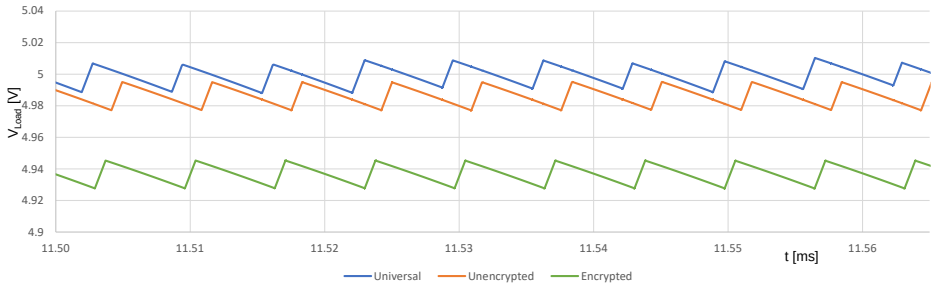


Figure 30. V_{Load} time graph curves using LM2594 regulator.

As a result of comparing the simulations, we can confirm that the differences between the official LM2594 models encrypted, unencrypted, and the universal model after applying parameters from the datasheet are negligible. The unencrypted model for LM2594 seems more stable than the previous LM2576HV model.

5. Discussion

Some producers provide a PSpice module for their products, but generally, there is a limited number of switched voltage regulator PSpice models. All the existing models are only equivalents for specific switching regulator and their typical properties. The customization of such models is minimal. A circuit simulation using "similar" but not equal values can lead to erroneous results. When a switched voltage regulator is used in practice, where the regulator does not have an equivalent PSpice model, it is impossible to rely on simulations.

The proposed and tested universal PSpice model of a switched voltage regulator is fully customizable. It is built on the basic principles of the switching voltage regulators shown in Figure 2 and allows any switching voltage regulator based on those principles to be simulated. It requires only the setup properties provided, usually from datasheets. Users do not have to depend on whether the manufacturer provides a PSpice model for their product to proceed with reliable simulations.

The paper aimed to present a universal PSpice model of the simple switcher such as LM2576, LM2596, LM 2577, etc. The buck DC–DC converter consists of a regulator switcher and other parts, where in addition to the switcher, the crucial are a coil and a capacitor as

an output filter. The paper's goal is not to design an optimal DC–DC buck converter with optimal values of the output filter parameters. The validation of the universal model is based on comparing the simulation results with other official models or real measurements under the same condition. Therefore, optimizing the output filter was not essential.

This paper showed that the universal model could be used as a full-fledged replacement for official simple regulator switcher simulation models of buck DC–DC converters. The simulation shows that the encrypted model has better and more stable results than the unencrypted model in the case of the LM2576HV model. The universal model shows results very close to the encrypted model. The only differences could be observed in the final voltage on the load, but according to the datasheet, the universal model is mathematically closer to the expected value.

A comparison with two different DC–DC regulators, LM2576 and LM2594, was performed. The LM2576 regulator was also compared with the real measurements and a dynamic load transient analysis. The presented universal PSpice model of a switched voltage regulator shows a very close match with the official model and also with the practically measured waveforms, even when it is adapted to various regulators. Generally, it cannot be claimed that the universal model is more accurate than the encrypted model provided by the manufacturers. Nevertheless, we can claim that the universal model is generally accurate level to the official encrypted models. It means that the universal model can be used as a simulation model in the TINA simulation software for the regulators, where only an encrypted model is provided or no official model exists at all. The universal model accuracy with the real regulator can be increased when the measurement of the element is performed. Then, the accurate parameters of the model could be calculated from the measurements. It would allow the user to simulate the regulator in different circumstances more accurately than the official models with constant parameters.

A significant advantage of our proposed model is that our model behavior could be more closely to real behavior when compared to official simulation models in a different situation. An example of such a situation could be, for instance, a simple parallel connection of the regulators. Equal current sharing can be observed when using official models, which is very unlikely, and it would be true only if the real regulator parameters were to be completely equal. However, slight parameter variation given by the manufacturer's tolerance is typically present between the different items of the same switching regulator type. These slight parameter differences could be set, or the parameter delay can be used using the universal model. It allows individual components to be customized if used multiple times in one circuit connection, and behavior can be more closely observed in a real situation.

Author Contributions: Conceptualization, D.K., T.V. and M.B.; methodology, I.K.; simulation software, T.V. and M.B.; validation, J.M. and J.D.; formal analysis, P.J.; writing—original draft preparation, D.K.; writing—review and editing, T.V.; visualization; supervision, D.K. and I.K. All authors have read and agreed to the published version of the manuscript.

Funding: This research received no external funding.

Data Availability Statement: The data presented in this study are available on request from the corresponding author. The data are not publicly available as the data also forms part of an ongoing study.

Acknowledgments: No acknowledgments.

Conflicts of Interest: The authors declare no conflict of interest.

Appendix A

The text notation of the model is built on PSpice model syntax [24,25], and it has the following form:

.SUBCKT 2576M Vin On_Off GND FB Vout PARAMS: f=52000 Uref=1.23 Imax=4.2 Rsw=0.019 Dmax=0.9 Vmax=40 Rint=8k Delay=10u; Name of sub-circuit and transmitted parameters

```
VA 12 60; Ammeter A
VS1 9 GND 5; Power supply + 5V
VG1 19 GND DC 0 AC 1 0; Frequency generator
+ PWL (0, 0) ({Delay} 0)
+ REPEAT FOREVER (0, 0)
+ (+10N 5)
+ (+{Dmax/f} 5)
+ (+10N 0)
+ (+10N 0)
+ (+{1/f-Dmax/f} 0)
+ (+10N 0)
+ ENDREPEAT
XU7 On_Off 6 GND 9 IC_7404_0; NOR1
XU5 7 6 8 GND 9 IC_7408_0; AND
SW3 9 10 FB GND S_VSWITCH_1; Voltage controlled switch 2
R2 GND 10 390; Resistor R
HCCVS1 11 GND VAM1 10; Conversion of switch S current to voltage
SW2 9 13 11 GND S_VSWITCH_2; Current control switch
R1 13 GND 390; Resistor R
S1 60 Vout Vin GND S_VSWITCH_4; Voltage controlled switch 1
S Vin 12 8 GND S_VSWITCH_3; Voltage controlled switch S
XU6 15 13 10 16 GND 9 IC_7427_0; NOR2
XU4 7 16 17 GND 9 IC_7400_0; R-S flip-flop
XU3 18 17 7 GND 9 IC_7400_0; R-S flip-flop
XU2 19 19 9 15 20 GND 9 IC_74121_0; Monostable flip-flop 2
XU1 GND GND 19 21 18 GND 9 IC_74121_0; Monostable flip-flop 1
Rint Vin GND {Rint}; Internal impedance
.MODEL S_VSWITCH_1 VSWITCH (RON=0 ROFF=1G VON={Vref} VOFF={Vref-0.000001})
.MODEL S_VSWITCH_2 VSWITCH (RON=0 ROFF=1G VON={10*Imax} VOFF={10*Imax-
0.01})
.MODEL S_VSWITCH_3 VSWITCH (RON={Rsw} ROFF=1G VON=1.8 VOFF=1.79)
.MODEL S_VSWITCH_4 VSWITCH (RON=0 ROFF=1000G VON={Vmax} VOFF={Vmax+0.1})
.ENDS
.SUBCKT IC_7404_0 1G 1A GND VCC
UNoname INV VCC GND 1G 1A U_SN7404_1 IO_STD
.MODEL U_SN7404_1 UGATE(TPLHTY=22N TPHLTY=15N)
.ENDS
.SUBCKT IC_7408_0 1G 1A 1B GND VCC
UNoname AND(2) VCC GND 1G 1A 1B U_SN7408_1 IO_STD
.MODEL U_SN7408_1 UGATE(TPLHTY=27N TPHLTY=19N)
.ENDS
.SUBCKT IC_7427_0 A B C D GND VCC
UNoname NOR(3) VCC GND A B C D U_SN7427_1 IO_STD
.MODEL U_SN7427_1 UGATE(TPLHTY=310N TPHLTY=350N)
.ENDS
.SUBCKT IC_7400_0 PRE_Neg J1 J2 GND VCC
UNoname NAND(2) VCC GND PRE_Neg J1 J2 U_SN7400_1 IO_STD
.MODEL U_SN7400_1 UGATE(TPLHTY=22N TPHLTY=15N)
.ENDS
.SUBCKT IC_74121_0 A1 A2 B Q Q_Neg GND VCC
UNoname INV VCC GND GND 31 U_SN7404_1 IO_STD
UNoname_2 NAND(2) VCC GND A1 A1 30 U_SN7400_1 IO_STD
UNoname_3 NAND(2) VCC GND 30 B 29 U_SN7400_2 IO_STD
UNoname_4 JKFF(1) VCC GND
```

```
+ 31 27 29 31 GND 23 24 U_SN7476_1 IO_STD
UNoname_5 INV VCC GND 29 28 U_SN7404_2 IO_STD
UNoname_6 NAND(2) VCC GND 28 23 25 U_SN7400_2 IO_STD
UNoname_7 JKFF(1) VCC GND
+ 23 31 25 GND 31 27 26 U_SN7476_2 IO_STD
UNoname_8 INV VCC GND 24 Q U_SN7404_2 IO_STD
UNoname_9 INV VCC GND 23 Q_Neg U_SN7404_3 IO_STD
.MODEL U_SN7404_1 UGATE(TPLHTY=22N TPHLTY=15N)
.MODEL U_SN7400_1 UGATE(TPLHTY=10N TPHLTY=10N)
.MODEL U_SN7400_2 UGATE(TPLHTY=0 TPHLTY=0)
.MODEL U_SN7476_1 UEFF(TPCLKQLHTY=35N TPCLKQHLTY=35N)
.MODEL U_SN7404_2 UGATE(TPLHTY=0 TPHLTY=0)
.MODEL U_SN7476_2 UEFF(TPCLKQLHTY=.69314718056N TPCLKQHLTY=.69314718056N)
.MODEL U_SN7404_3 UGATE(TPLHTY=5N TPHLTY=5N)
.ENDS
```

References

1. Bereš, M.; Kováč, D.; Vince, T.; Kováčová, I.; Molnár, J.; Tomčíková, I.; Dziak, J.; Jacko, P.; Fecko, B.; Gans, Š. Efficiency Enhancement of Non-Isolated DC-DC Interleaved Buck Converter for Renewable Energy Sources. *Energies* **2021**, *14*, 4127. [CrossRef]
2. Hafeez, K.T.; Dutta, A.; Singh, S.G.; Avalur, K.K.G. A low-cost multi-phase 3A buck converter with improved ripple cancellation for wide supply range. In Proceedings of the 2016 IEEE International Symposium on Circuits and Systems (ISCAS), Montreal, QC, Canada, 22–25 May 2016; pp. 1618–1621. [CrossRef]
3. Bereš, M.; Schweiner, D.; Kováčová, I.; Kalinov, A. Current Ripple Comparison of Multi and Single Phase Buck-Boost Converters. In Proceeding of the MEES'17, Kremenchuk, Ukraine, 15–17 November 2017; pp. 260–263.
4. de Souza, A.F.; Tofoli, F.L.; Ribeiro, E.R. Switched Capacitor DC-DC Converters: A Survey on the Main Topologies, Design Characteristics, and Applications. *Energies* **2021**, *14*, 2231. [CrossRef]
5. Mobayen, S.; Bayat, F.; Lai, C.-C.; Taheri, A.; Fekih, A. Adaptive Global Sliding Mode Controller Design for Perturbed DC-DC Buck Converters. *Energies* **2021**, *14*, 1249. [CrossRef]
6. Liu, P.-J.; Kuo, M.-H. Adaptive On-Time Buck Converter with Wave Tracking Reference Control for Output Regulation Accuracy. *Energies* **2021**, *14*, 3809. [CrossRef]
7. Roh, Y.S.; Moon, Y.J.; Park, J.; Jeong, M.G.; Yoo, C. A multiphase synchronous buck converter with a fully integrated current balancing scheme. *IEEE Trans. Power Electron.* **2015**, *30*, 5159–5169. [CrossRef]
8. Parvez, M.; Pereira, A.T.; Ertugrul, N.; Weste, H.E.; Abbott, D.; Al-Sarawi, S.F. Wide Bandgap DC–DC Converter Topologies for Power Applications. *Proc. IEEE* **2021**, *109*, 1253–1275. [CrossRef]
9. Morcillo Bastidas, J.D.; Muñoz, J.G.; Olivar Tost, G. Simulation and Analysis of Complex Behaviors in a DC-DC Buck Converter. *IEEE Lat. Am. Trans.* **2021**, *19*, 68–74. [CrossRef]
10. Park, D.-R.; Kim, Y. Design and Implementation of Improved High Step-Down DC-DC Converter for Electric Vehicles. *Energies* **2021**, *14*, 4206. [CrossRef]
11. Texas Instruments. Datasheet LM2576. Available online: https://www.ti.com/lit/ds/symlink/lm2576.pdf (accessed on 16 February 2021).
12. Texas Instruments. Datasheet LM2574. Available online: https://www.ti.com/lit/ds/snvs104f/snvs104f.pdf (accessed on 16 February 2021).
13. Martin, K.; Pavlík, M.; Kolcun, M. The impact of multi-system overhead lines operation with different voltage levels to voltage unbalance. *Elektroenergetika* **2015**, *2015*, 73–76.
14. Kováč, D.; Kováčová, I.; Schweiner, D. Wiring for Extending the Current and Voltage Load Capacity of a Switched Voltage Regulator. Patent Application No. 00129-2019, 2019.
15. Lin, J.-Y.; Hsu, Y.-C.; Lin, Y.-D. A Low EMI DC-DC Buck Converter with a Triangular Spread-Spectrum Mechanism. *Energies* **2020**, *13*, 856. [CrossRef]
16. Rashid, H. Muhammad. In *Power Electronics Handbook*; Elsevier Inc.: Amsterdam, The Netherlands, 2011; ISBN 978-0-12-382036-5.
17. Kovacova, I.; Kovac, D. Electromagnetic coupling—EMC of Electrical Systems. *J. Commun. Antenna Propag.* **2014**, *4*, 51–57.
18. Xu, W.; Fang, J.; He, J.; Kim, T. Switching voltage regulator modeling and its applications in power delivery design. In Proceedings of the IEEE International Symposium on Electromagnetic Compatibility (EMC), Raleigh, NC, USA, 4–8 August 2014; pp. 855–860. [CrossRef]
19. Texas Instruments. PSpice-For-Ti, PSpice®for TI Design and Simulation Tool. Available online: https://www.ti.com/tool/PSPICE-FOR-TI (accessed on 16 March 2021).

20. Texas Instruments. TINA-TI, PSpice®for TI Design and Simulation Tool. Available online: https://www.ti.com/tool/TINA-TI (accessed on 16 March 2021).
21. Cadence Design Systems, Inc. *PSpice Reference Guide, Reference Guide Second Online Edition*; Cadence Design Systems, Inc.: San Jose, CA, USA, 2000; 374p.
22. Fitzpatrick, D. *Analog Design and Simulation Using OrCAD Capture and PSpice*; Elsevier: Newnes, Australia, 2017.
23. PSpice User Manual. Available online: https://www.academia.edu/36059575/PSpice_User_Manual (accessed on 14 October 2020).
24. Zbojovský, J.; Kruželák, L.; Pavlík, M. Impedance Spectroscopy of Liquid Insulating Materials. In Proceedings of the 2018 International IEEE Conference and Workshop in Óbuda on Electrical and Power Engineering (CANDO-EPE), Budapest, Hungary, 2–21 November 2018; pp. 000249–000254. [CrossRef]
25. Pavlík, M.; Kolcunová, I.; Lisoň, L. Measuring the shielding effectiveness and reflection of electromagnetic field of building material. In Proceedings of the 2015 16th International Scientific Conference on Electric Power Engineering (EPE), Kouty nad Desnou, Czech Republic, 20–22 May 2015; pp. 56–59. [CrossRef]
26. Texas Instruments. LM2576HV, Active Simple Switcher®4V to 60V, 3A Low Component Count Step-Down Regulator. Available online: https://www.ti.com/product/LM2576HV (accessed on 14 March 2022).
27. Vince, T.; Beres, M.; Kovacova, I.; Molnar, J.; Fecko, B.; Dziak, J.; Tomcikova, I.; Guzan, M. IoT Implementation in Remote Measuring Laboratory VMLab Analyses. *J. Univers. Comput. Sci.* **2020**, *26*, 1495–1512. [CrossRef]
28. Texas Instruments. LM2594HV, SIMPLE SWITCHER Power Converter 150 kHz 0.5A Step-Down Voltage Regulator. Available online: https://www.ti.com/product/LM2594HV (accessed on 10 May 2022).